

S. James and M. S. Anand
Rolls-Royce
P. O. Box 420, Speed Code T-14
Indianapolis, IN 46206
and
S. B. Pope
Sibley School of Mechanical and Aerospace Engineering
Cornell University
Ithaca, NY 14853

ABSTRACT

Probability density function (PDF) transport methods are increasingly used in simulations of gas turbine combustors. One of the main advantages of the PDF transport method is that the crucial turbulence-chemistry interaction is accurately accounted for. Due to its large dimensionality, the PDF transport equation is solved using one of two Monte-Carlo methods – the Eulerian (or node-based) method and the Lagrangian method. Studies on the Eulerian method show that a large number of particles per cell is necessary for accurate simulations. In the present study, the Lagrangian method is developed for the simulation of actual gas turbine combustors. The key technologies developed are a robust particle tracking algorithm and a variable time-step algorithm to accelerate the convergence of the flow. The accuracy of the Lagrangian method is evaluated by applying it to several combustor configurations. A model combustor and two production combustors are studied. The predicted exit temperature profiles are in excellent agreement with rig data. Simulations show that even with 10 particles per cell, accurate results are obtained. The study shows that the Lagrangian Monte-Carlo PDF method can be reliably used in simulations of practical gas turbine combustors.

INTRODUCTION

With increasing emphasis on accurate CFD predictions of the flow in gas turbine combustors, there is greater need to develop advanced models. Predicting the combusting flow in gas turbine combustors is a complex task due to the strong role played by turbulence-chemistry interactions. The traditional approach to modeling these interactions via the eddy-dissipation model or the presumed PDF model has met with limited success. In light of this, the PDF transport method^{1,2} is a promising alternative to modeling turbulent-chemistry interactions. Several

studies have shown that this method can accurately predict turbulent flames, even flames close to extinction³⁻⁶. There have been several studies of PDF methods in axisymmetric reacting flow configurations. However, studies in three-dimensional flow configurations have been limited due to the difficulty of solving the PDF transport equation in complex three-dimensional flows^{7,8}.

In the present study, the joint PDF of scalars (or composition) is considered, as opposed to the more comprehensive and computationally intensive velocity-scalar-dissipation PDF method^{3,4}. The PDF transport equation is a hyperdimensional equation and is generally solved using Monte-Carlo methods. In Monte-Carlo methods, an ensemble of particles represents the joint PDF of scalars. The transport of these particles in physical and compositional space mimics the solution of the transport equation. In the Eulerian Monte-Carlo method, all the particles in a cell are located at the cell-center. The transport of these particles is determined by cell-face fluxes, computed from the flowsolver. An accompanying study⁷ on the application of the Eulerian method for gas turbine combustors showed that a large number of particles per cell is required for accurate simulations. Studies⁹ in 2D flows have shown that for a given accuracy level, the Lagrangian Monte-Carlo scheme is cheaper than the Eulerian scheme. In the Lagrangian Monte-Carlo method, particles are randomly distributed in the computational domain and are associated with the cell that they are in at a given instant of time. The implementation of the Lagrangian method is significantly more complex than the Eulerian method; hence, there have been few applications of the Lagrangian method to complex three-dimensional flows. The main difficulty in the method is the accurate tracking of particles and conservative implementation of various submodels. In the present study, the Lagrangian method has been developed for the simulation of the flow in gas turbine combustor configurations. The key technologies developed in the method are a robust particle tracking algorithm, accurate treatment of boundary conditions, and a conservative

Copyright © 2002 by Rolls-Royce Corporation and Cornell University. Published by AIAA, Inc., with permission.

implementation of molecular mixing and spray evaporation. A variable time-stepping scheme has also been developed to accelerate the convergence of the solution.

The Monte-Carlo solution method involves the integration of the chemical rate equations on each particle. In direct integration (DI), the smallest reaction time-scale is resolved and the rate equations are directly integrated – a computationally expensive method. In the table look-up algorithm, an a priori integration table is created before the start of the CFD calculation. During the CFD calculation, linear interpolations of the tabulated values are performed to integrate the rate equations. In the intrinsic low-dimensional manifold (ILDm) method¹⁰, a reduced manifold consisting of one or two scalars describes the chemical reactions. This manifold is created a priori and accessed during the CFD calculation. In the in-situ adaptive tabulation (ISAT) method¹¹, a reaction table is created dynamically as the CFD calculation progresses. The table look-up method is suitable for reaction mechanisms with few numbers of scalars and reaction steps. The ILDM method reduces the detailed chemical mechanism to a smaller reaction mechanism; as a result, the number of degrees of freedom of the reaction mechanism is significantly reduced. The ISAT method is the most desirable for accurately integrating large reaction mechanisms.

In the next section, the PDF transport equation is presented followed by a discussion on the Lagrangian Monte-Carlo solution methodology. A description of the combustion chemistry and spray models is also presented in this section. Calculations of gas turbine combustors are presented in the results and discussions section. The conclusions of the study are reported in the summary section.

FORMULATION

The PDF transport equation is used in conjunction with a finite-volume solver, PRECISE¹², which solves for the velocity, pressure, and turbulence fields. A pressure-correction algorithm is used to compute the velocity and pressure fields. The turbulence fields are obtained by solving the conventional $k-\varepsilon$ equations. The finite-volume solver employs a second-order accurate Hybrid Linear/Parabolic Approximation (HLPa) scheme¹³ to compute the convective terms. The PDF transport equation is solved once every flow iteration until the overall flowfield converges. The density is obtained from the PDF module and is the main link between the finite-volume solver and the PDF solver. The velocities necessary for solving the PDF equation are obtained from the finite-volume module.

The PDF Transport Equation

The starting point for the derivation of the scalar PDF transport equation is the instantaneous

continuity and species/enthalpy transport equations, given below.

$$\frac{\partial \rho}{\partial t} + \frac{\partial}{\partial x_i} (\rho u_i) = \rho m_0 \quad (1)$$

$$\frac{\partial}{\partial t} (\rho \phi_\alpha) + \frac{\partial}{\partial x_i} (\rho u_i \phi_\alpha) = -\frac{\partial J_i^\alpha}{\partial x_i} + \rho S_\alpha + \rho m_\alpha \quad (2)$$

In the above equations, ρ is the density, u_i is the instantaneous velocity, J_i^α is the diffusional flux, ϕ_α represents the mass fraction of species α or enthalpy, $S_\alpha(\phi)$ is the chemical source term for species α , ρm_0 is the mass source term due to fuel evaporation and $m_\alpha (= m_0 c_\alpha)$ is the rate of change of mass fraction of species α due to fuel evaporation. c_α is the mass fraction of species α in the fuel vapor. For the enthalpy scalar, c_α denotes the enthalpy of the evaporated fuel. From Equations (1) & (2), the governing equation for the transport of the mass density function $F(\underline{\psi}, \underline{x}; t)$ is given by:

$$\begin{aligned} \frac{\partial}{\partial t} (F) + \frac{\partial}{\partial x_i} (U_i F) &= \frac{\partial}{\partial \psi_\alpha} \left\langle \left(\frac{1}{\rho} \frac{\partial}{\partial x_i} J_i^\alpha \right) \middle| \underline{\psi} \right\rangle F \\ &- \frac{\partial}{\partial x_i} \langle u_i'' | \underline{\psi} \rangle F - \frac{\partial}{\partial \psi_\alpha} (S_\alpha F) \\ &- \frac{\partial}{\partial x_i} \langle (m_\alpha - m_0 \phi_\alpha) | \underline{\psi} \rangle F + \langle m_0 | \underline{\psi} \rangle F. \end{aligned} \quad (3)$$

In this equation, $\underline{\psi}$ is the scalar vector, U_i is the Favre mean velocity, and u_i'' is the fluctuating velocity. The symbol $\langle A | B \rangle$ is the expected value of A conditioned on B . The terms on the left-hand side are the rate of change of the PDF and the convection of the PDF. The first term on the right-hand side is the molecular mixing term. The second term on the right-hand side is the turbulent convection of the PDF in physical space. The third term is the effect of chemical reactions on the PDF in compositional space. The fourth and the fifth terms are the effect of spray evaporation on the PDF. Note that no modeling is required for the chemical reaction term. Thus, chemical reactions of arbitrary complexity can be exactly evaluated. The terms that require modeling are the molecular mixing, turbulent convection terms and the spray evaporation terms.

Modeling

The molecular mixing term is modeled by the interaction by exchange with the mean (IEM) model¹⁴ given by:

$$\frac{\partial}{\partial \psi_\alpha} \left(\left\langle \frac{1}{\rho} \frac{\partial J_i^\alpha}{\partial x_i} \middle| \underline{\psi} \right\rangle F \right) = \frac{\partial}{\partial \psi_\alpha} [C_\phi \omega (\psi_\alpha - \langle \phi_\alpha \rangle) F] \quad (4)$$

The model constant C_ϕ has a value of 2.0. The mixing frequency ω is expressed in terms of turbulent kinetic energy k and turbulent dissipation ε ($\omega = \varepsilon/k$). The turbulent convection term is modeled by the gradient diffusion model² and is given by:

$$\langle u_i^n | \underline{\psi} \rangle F = -\langle \rho \rangle D_t \frac{\partial}{\partial x_i} \left(\frac{F}{\langle \rho \rangle} \right), \quad (5)$$

where, $D_t (= \nu_t / Sc_t)$ is the turbulent diffusivity and expressed in terms of the turbulent kinematic viscosity ν_t and the turbulent Schmidt number Sc_t .

Now consider the spray evaporation terms in Equation (3). Spray is modeled by inserting fuel vapor particles, each particle having a fixed fuel composition \underline{c} , into the flowfield. This leads to the expressions:

$$\begin{aligned} \langle m_0 | \underline{\psi} \rangle &= m_0, & \underline{\psi} &= \underline{c} \\ &= 0, & \underline{\psi} &\neq \underline{c} \end{aligned} \quad (6)$$

and,

$$\frac{\partial}{\partial \psi_\alpha} \left[\langle (m_\alpha - m_0 \phi_\alpha) | \underline{\psi} \rangle F \right] = 0 \quad (7)$$

The final modeled form of the PDF transport equation is:

$$\begin{aligned} \frac{\partial}{\partial t} (F) + \frac{\partial}{\partial x_i} (U_i F) &= \frac{\partial}{\partial \psi_\alpha} (C_\phi \omega (\psi_\alpha - \langle \phi_\alpha \rangle) F) \\ &+ \frac{\partial}{\partial x_i} \left(\langle \rho \rangle D_t \frac{\partial}{\partial x_i} \left(\frac{F}{\langle \rho \rangle} \right) \right) - \frac{\partial}{\partial \psi_\alpha} (S_\alpha F) \\ &+ \langle m_0 | \underline{\psi} = \underline{c} \rangle F. \end{aligned} \quad (8)$$

Monte-Carlo Method

Consider the discrete mass density function $F_n(\underline{\psi}, \underline{x}; t)$ represented by an ensemble of N notional particles, each having mass $\Delta m \cdot w^n$, position \underline{x}^n and scalar values $\underline{\phi}^n$. w^n is the weight of a particle. F_n can be defined as:

$$F_n(\underline{\psi}, \underline{x}; t) = N \Delta m \langle w^n \delta(\underline{\psi} - \underline{\phi}^n) \delta(\underline{x} - \underline{x}^n) \rangle. \quad (9)$$

It can be shown² that the evolution equation for the Lagrangian system defined as,

$$\begin{aligned} \Delta \underline{x}^n(t) &= D(\underline{x}^n[t], t) \delta t + [B(\underline{x}^n[t], t)]^{1/2} \Delta \underline{W}_t \\ \Delta \underline{\phi}^n(t) &= -C_\phi \omega (\underline{\phi}^n - \langle \underline{\phi}^n \rangle) \delta t + \underline{S} \delta t, \end{aligned} \quad (10)$$

where,

$$\begin{aligned} \underline{D} &= \underline{U} + \frac{1}{\langle \rho \rangle} \nabla \langle \rho \rangle D_t \\ B &= 2D_t \\ \Delta \underline{W}_t &= \delta t^{1/2} \underline{\xi} \end{aligned} \quad (11)$$

$\underline{\xi}$ = Standardized joint normal random vector,

mimics the transport of F ; i.e., the transport equation of F_n derived from Equations (10) and (11) has the same form as Equation (8) sans the spray evaporation term. The mean flow parameters needed in Equation (10) are computed via a trilinear interpolation scheme in computational space.

Spray Evaporation

Consider the last term on the r.h.s. of Equation (8).

$$\frac{\partial}{\partial t} (F) = \langle m_0 | \underline{\psi} = \underline{c} \rangle F. \quad (12)$$

This equation can also be written as:

$$\frac{\partial}{\partial t} (F) = \langle m_0 \rangle f^s(\underline{c}, \underline{x}; t), \quad (13)$$

where, $\langle m_0 \rangle$ is the unconditioned evaporation rate and $f^s(\underline{c}, \underline{x}; t)$ is the mass density function of the new vapor.

Considering the discrete mass density function, let n be the number of particles created per unit time from the new vapor and let w^v be the weight of each added vapor particle. Then,

$$F_n(t + \delta t) = F_n(t) + n \Delta m \delta t w^v \langle \delta(\underline{\psi} - \underline{c}) \delta(\underline{x} - \underline{x}^n) \rangle. \quad (14)$$

This can be further written as

$$\frac{\partial F_n}{\partial t} = \frac{n}{N_0} N_0 \Delta m w^v \langle \delta(\underline{\psi} - \underline{c}) \delta(\underline{x} - \underline{x}^n) \rangle. \quad (15)$$

where, N_0 is the number of particles (each having weight w^v) representing the fuel vapor mass density function. Comparing Equations (13) and (15), it can be deduced that the two equations are equivalent if:

$$n = N_0 \langle m_0 \rangle, \quad (16a)$$

$$N_0 \Delta m w^v \langle \delta(\underline{y} - \underline{c}) \delta(\underline{x} - \underline{x}^n) \rangle = f^s(\underline{c}, \underline{x}; t). \quad (16b)$$

For a computational cell k with volume ∇_k , it can be shown from Equation (16b) that:

$$N_o = \frac{\rho^{vapr} \nabla_k}{w^v \Delta m}. \quad (17)$$

Thus, Equation (16a) can be rewritten as:

$$w^v = \frac{\rho^{vapr} \nabla_k}{n \Delta m} \langle m_0 \rangle. \quad (18)$$

By assuming a fixed value for the number of vapor particles inserted into the cell (i.e. $n \Delta t = \text{fixed}$), the weight of each of these particles (with composition \underline{c}) can then be computed from Equation (18).

Particle Tracking

The objective of the particle tracking algorithm is to determine the cell index associated with the final position of a particle after the convection and diffusion processes. A cell is defined by eight vertices. Each face of the six cell faces is bounded by the four straight-line segments connecting the four vertices of the face. In general, these four vertices are not coplanar, and hence a cell face cannot be considered to be a plane. Instead, a face is considered to be made up of two triangles. A cell is, therefore, bounded by the closed, connected surface consisting of 12 triangles.

Let T denote a general triangle (Figure 1). We then define: P to be the plane containing T , \underline{n} the normal to T (pointing out of the cell), and \underline{p} any point in P . We consider a particle initially located at \underline{y} and moving with a constant velocity \underline{u} . Hence at time t , its position is given by

$$\underline{x}(t) = \underline{y} + \underline{u}t. \quad (19)$$

The trajectory $\underline{y} \rightarrow \underline{x}$ intersects P if $\underline{u} \cdot \underline{n} > 0$. Such an intersection occurs at time

$$t^* \equiv (\underline{p} - \underline{y}) \cdot \underline{n} / \underline{u} \cdot \underline{n}. \quad (20)$$

On average, the trajectory interests 6 of the 12 planes. We refer to this type of intersection as an ‘‘outcrossing’’, characterized by $\underline{u} \cdot \underline{n} > 0$. An outcrossing can be followed by (one or more) ‘‘incrossings’’ and ‘‘outcrossings’’, the incrossings characterized by $\underline{u} \cdot \underline{n} < 0$. We want to determine the first cell boundary crossing, which is inevitably an

outcrossing: hence we do not need to consider incrossings. The point of intersection

$$\underline{x}^* \equiv \underline{x}(t^*) = \underline{y} + \underline{u}t^*. \quad (21)$$

may or may not fall within the triangle T . The cell outcrossing is the first intersection of $\underline{x}(t)$ with a triangle. The particle trajectory intersects the cell face containing this triangle and passes through the cell adjacent to this face. The above algorithm of determining the face intersected by the particle trajectory is then applied to this cell. This procedure is continued until a cell is identified where the particle trajectory does not intersect any of the cell’s outcrossing faces. This is the cell associated with the final particle position.

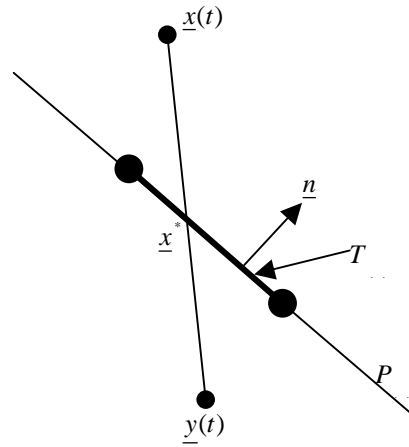


Figure 1. Illustration of a particle crossing a surface.

Molecular Mixing

The IEM mixing model is implemented as in Jenny *et al.*¹⁵ For a particle with composition $\phi_\alpha^n(t)$, position \underline{x}^n and weight w^n , the model is defined as:

$$d\phi_\alpha^n = -0.5C_\phi \omega (\phi_\alpha^n - \langle \phi_\alpha^n \rangle) dt. \quad (22)$$

In the above equation, $\langle \phi_\alpha^n \rangle$ is the mean scalar value at the location of particle n . This value is not the same as that obtained by computing the ensemble mean of scalar values within the cell containing the particle. The essence of the implementation is to specify a valid numerical approximation $\hat{\phi}_\alpha^n$ to $\langle \phi_\alpha^n \rangle$. Let F_α^c be the value of $\hat{\phi}_\alpha^n$ at a corner c of the cell containing the particle n . Let \hat{g}_c be the linear basis function coefficient, so that interpolation from corners to the particle position is expressed by:

$$\hat{\phi}_\alpha^n = \sum_c \hat{g}_c(\underline{x}^n) F_\alpha^c. \quad (23)$$

From the above definition and the requirement that the implementation of the model be conservative, the following expression for F_α^c can be derived¹⁵.

$$F_\alpha^c = \frac{\sum_n \hat{g}_c(\underline{x}^n) w^n d^n \phi_\alpha^n}{\sum_n \hat{g}_c(\underline{x}^n) w^n d^n}, \quad (24)$$

where, $d^n = 1 - \exp(-0.5C_\phi \omega \Delta t)$.

Variable Time-Step

A variable time-step algorithm for the transport of particles can significantly accelerate the convergence of the flowfield. This algorithm within the context of the joint velocity-scalar PDF method was derived in Muradoglu and Pope¹⁶. Here, we present the algorithm for the joint scalar PDF method.

The local time-step in each cell is determined by the Courant number condition. Since the time-step varies from one cell to the next, the stochastic differential equations [Equation (10)] have to be reformulated.

Consider the standard uniform time-step equation:

$$\Delta \underline{x}^n(t) = D(\underline{x}^n[t], t) \delta t + [B(\underline{x}^n[t], t)]^{1/2} \Delta W_i. \quad (25)$$

We consider the statistically stationary case, so that the coefficients do not depend on time. The evolution equation for the mass density function

$G(\underline{x}; t) = \langle m \delta(\underline{x}^n(t) - \underline{x}) \rangle$, where m is the total mass in the system, corresponding to Equation (25) is given by:

$$\frac{\partial G}{\partial t} = -\frac{\partial}{\partial x_i} (D_i(\underline{x})G) + \frac{\partial^2}{\partial x_i \partial x_i} (B(\underline{x})G). \quad (26)$$

With variable time-step, we define,

$$\hat{G}(\underline{x}; s) = \langle m w^n(s) \delta(\underline{x}^n(s) - \underline{x}) \rangle, \quad (27)$$

where, s is a pseudo-time, and specify the particle evolution equations as,

$$\begin{aligned} \Delta \underline{x}^n(s) &= D(\underline{x}^n[s]) \gamma \Delta s + [2\gamma B(\underline{x}^n[s])]^{1/2} \Delta W_i \\ d \left[\frac{w^n(s)}{\gamma(\underline{x}^n(s))} \right] &= 0, \end{aligned} \quad (28)$$

where, $\gamma(\underline{x}) = \Delta t(\underline{x}) / \Delta s$ is a specified positive field. From the above equations, we have,

$$dw^n(s) = \xi d\gamma[\underline{x}^n(s)], \quad (29)$$

where, $\xi = w^n(0) / \gamma(\underline{x}^n(0))$ is a fixed constant for each particle. The evolution of $\hat{G}(\underline{x}; s)$ can be derived as follows.

$$\begin{aligned} \hat{G}(\underline{x}; s + \Delta s) &= \langle m w^n(s + \Delta s) \delta(\underline{x}^n(s + \Delta s) - \underline{x}) \rangle \\ &= \langle m \xi \gamma(\underline{x}^n + d \underline{x}^n) \delta(\underline{x}^n - \underline{x} + d \underline{x}^n) \rangle \\ &= \left\langle m \xi \left(\gamma + \frac{\partial \gamma}{\partial x_i} dx_i^n + \frac{1}{2} \frac{\partial^2 \gamma}{\partial x_i \partial x_i} dx_i^n dx_i^n \right) \times \right. \\ &\quad \left(\delta(\underline{x}^n - \underline{x}) - \frac{\partial}{\partial x_k} \delta(\underline{x}^n - \underline{x}) dx_k^n + \right. \\ &\quad \left. \left. \frac{1}{2} \frac{\partial^2}{\partial x_k \partial x_i} \delta(\underline{x}^n - \underline{x}) dx_k^n dx_i^n \right) \right\rangle \end{aligned} \quad (30)$$

Further simplification yields:

$$\begin{aligned} \hat{G}(\underline{x}; s + \Delta s) &= \hat{G}(\underline{x}; s) + \hat{G} \frac{\partial \gamma}{\partial x_i} D_i ds + \\ &\frac{1}{2} \hat{G} \frac{\partial^2 \gamma}{\partial x_i \partial x_j} 2B ds \delta_{ij} - \frac{\partial}{\partial x_k} (\hat{G} D_k \gamma ds) + \\ &\frac{1}{2} \frac{\partial^2}{\partial x_k \partial x_i} (\hat{G} 2B \gamma ds \delta_{ki}) - \frac{\partial}{\partial x_k} \left(\hat{G} \frac{\partial \gamma}{\partial x_i} 2B ds \delta_{ik} \right) \end{aligned} \quad (31)$$

which can be further reduced to

$$\frac{1}{\gamma} \frac{\partial}{\partial s} (\hat{G}) = -\frac{\partial}{\partial x_i} (\hat{G} D_i) + \frac{\partial^2}{\partial x_i \partial x_i} (\hat{G} B). \quad (32)$$

For stationary flows, the l.h.s. of the equation is zero and the above equation becomes identical to the stationary form of Equation (26). The particle equation in composition space can be shown to be

$$\Delta \phi^n(s) = -C_\phi \omega (\phi^n - \langle \phi^n \rangle) \gamma \Delta s + S \gamma \Delta s. \quad (33)$$

Equations (28) and (33) constitute the variable time-step particle evolution equations. The weight w^n at the end of the timestep Δs is computed as

$$w^n(s + \Delta s) = w^n(s) \frac{\gamma(\underline{x}^n(s + \Delta s))}{\gamma(\underline{x}^n(s))}. \quad (34)$$

Particle weights are prevented from becoming excessively large or small by a process of ‘‘cloning’’ and ‘‘clustering’’. Particles below a certain weight are combined into one particle, while particles above a certain weight are split into multiple particles. This is

done to ensure that particles within a cell have more or less uniform weights.

Combustion Chemistry

The fuels used in the simulations are Propane and Jet A. A two-step generalized Westbrook and Dryer scheme¹⁷ is used to represent the combustion chemistry. In addition to fuel and oxygen, the other scalars involved in the combustion process are CO₂, H₂O, CO and N₂. The integration of the chemical source term is achieved using the table look-up method. The results of the a priori integration are stored in the form of tables. During the CFD calculation, the tables are accessed and linear interpolation is performed to determine the change in composition due to reaction. The tables are parameterized by mixture fraction, CO₂, H₂O and timestep in the two-step mechanism. For the two-step mechanism, given the values of mixture fraction, CO₂ and H₂O, the remaining species can be computed using algebraic relations.

Spray Transport

The liquid fuel spray is assumed to be composed of a large number of spray droplets of different sizes. These droplets are transported using a Lagrangian model^{18,19}. The model is described by the equations:

$$\begin{aligned} dx_i^d &= u_i^d dt \\ dU_i^d &= \frac{u_i - u_i^d}{\tau_d} dt + g_i dt, \end{aligned} \quad (35)$$

where, u_i is the instantaneous fluid velocity at the droplet location, u_i^d is the droplet velocity, g_i is the acceleration due to gravity, and τ_d is the droplet dynamic relaxation time. The instantaneous fluid velocity is sampled from the assumed independent Gaussian distribution. The value of the relaxation time is chosen as the minimum of the turbulent eddy lifetime and the residence time of the particle in the eddy. As the droplets move through the flowfield, they evaporate. The governing equations for heat and mass balance are solved iteratively to compute the evaporated mass over the period of the droplet timestep, such that the heat and mass balances are satisfied²⁰. The evaporated fuel and the corresponding enthalpy are added as source terms in the PDF transport equation. Additionally, the momentum exchange between droplets and the surrounding flow are also accounted for as source terms in the flow equations.

RESULTS AND DISCUSSIONS

In this section, results from PDF simulations of three gas turbine combustors are presented. The combustors will be denoted as A, B and C.

Combustor-A employs gaseous fuel, while Combustors-B & C employ liquid fuel.

Combustor-A

A model combustor with gaseous Propane fuel is first studied. A schematic of the combustor is presented in Figure 2. The simulated flow domain is a 22-degree sector of an annular combustor. The system pressure and temperature of the flows are 14.8 atm and 735 K, respectively. Gaseous Propane flows through a fuel nozzle at the center of the dome. An air swirler surrounds this nozzle. A total of 43,000 nodes are used to represent the geometry.

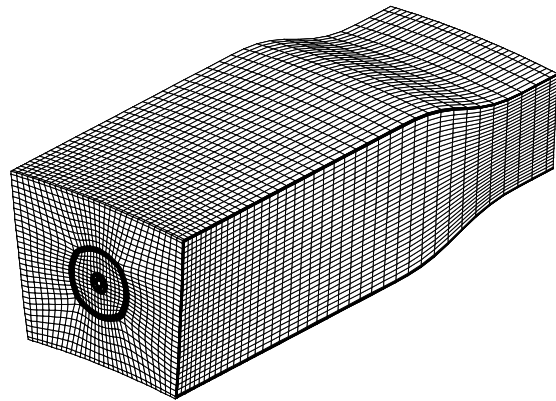


Figure 2. The grid used in the simulation of Combustor-A. Gaseous Propane fuel is injected from a fuel nozzle at the center of the inlet plane. An air swirler surrounds the fuel injection location.

Two PDF simulations are performed – with 10 particles per cell and with 60 particles per cell (values at start of the calculations). The two simulations can be analyzed to assess the statistical and bias errors in the PDF algorithm. A cold flow simulation is first performed until the mixture fraction field is sufficiently evolved. Subsequently, an ignition source is introduced in the recirculating zone for ten iterations. The simulation is then continued until steady-state is reached and the average mixture fraction value at the exit of the combustor match the theoretical value of 0.0355, computed from the mass flow rates of air and fuel entering the combustor. Figure 3 shows the u-velocity field on a plane passing through the center of the fuel nozzle, swirler and liner walls (center k-plane) in the combustor. A recirculating zone is seen in the combustor. The recirculating zone acts as an anchor for the flame and helps to stabilize the reacting front. This stabilization of the flame is seen in Figure 4, which shows the temperature field in the combustor from the two simulations. The overall flame structure looks similar in the two simulations. Minor differences are seen in the high temperature region at the flame anchoring

location. Downstream of this location, the flame shows a “necking” effect, suggesting the importance of finite-rate chemistry effects in this region.

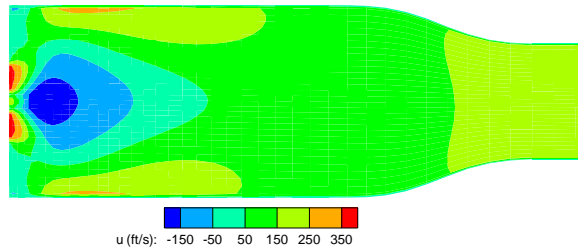


Figure 3. The u -velocity field at the center k -plane of the combustor. A recirculating region is observed close to the dome.

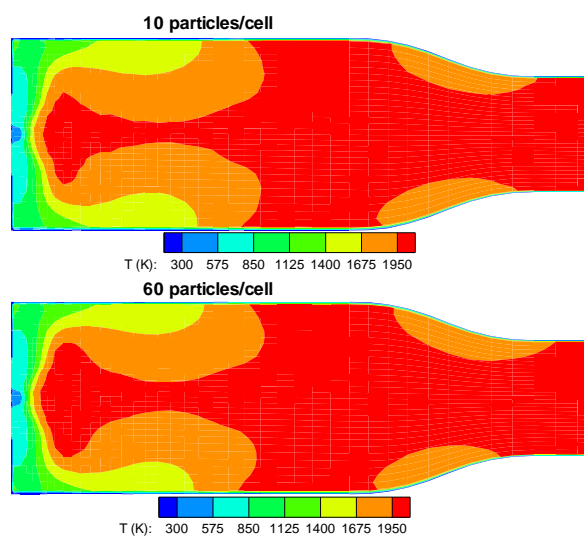


Figure 4. The temperature field in the combustor from PDF calculations with 10 (top) particles per cell and 60 (bottom) particles per cell.

Figure 5 shows the evolution of mixture fraction and temperature at the center of the combustor where the cross-sectional area starts decreasing. The two simulations are ignited at different times; hence the temperature rise is different in the two cases. The procedure of time-averaging the mean fields computed from particles is used in the simulations to reduce statistical fluctuations. It can be seen that the two simulations converge to the same value in both mixture fraction and temperature fields. Note that statistical fluctuations in mixture fraction during initial times with 10 particles per cell are quite high. The fluctuations are substantially lower with 60 particles per cell.

The time evolution of the total number of particles (not shown) shows an initial transient. Subsequently, the total number of particles settles to a steady value at convergence. In the two simulations, the final number of particles per cell, on an average,

is 10.5 and 65.7. It is also noted that fluctuations in the total number of particles in the flow domain are higher with 10 particles per cell. The minor differences in the two simulations indicate that bias errors are small. This is an encouraging result, as simulations with as low as 10 particles per cell can be performed thus significantly saving valuable CPU time and memory. Detailed analyses of errors in transport PDF algorithms are presented in Xu and Pope²¹.

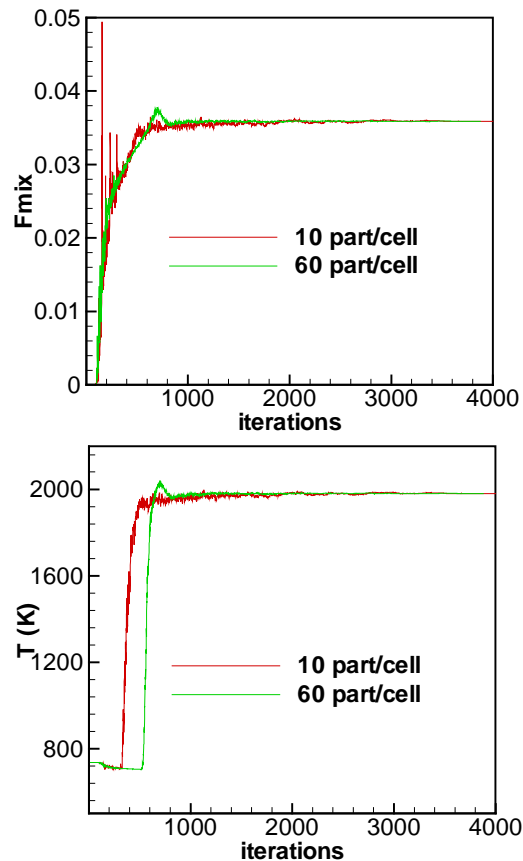


Figure 5. Evolution of mixture fraction (top) and temperature (bottom) with 10 particles per cell and 60 particles per cell. Note that converged results are independent of the number of particles per cell used in the simulations.

Combustor-B

Combustor-B is a variant of a production gas turbine combustor. Simulation of the flow in this combustor is a stringent test for the predictive capability of the PDF methodology and the feasibility of performing PDF transport calculations of real engine combustors.

Figure 6 shows the combustor grid used in the PDF simulations. The combustor is operated at a pressure of 18 atm and a temperature of 782 K. Air flows through two swirlers on the dome, and primary, dilution and effusion holes on the liner. Simulations are performed on a grid with 400,752 nodes and with

10 particles per cell. In order to assess the capability of the PDF method to handle flows in practical gas turbine combustors, a simulation of Combustor-B with gaseous Propane fuel is first performed. This simulation will allow an assessment of the accuracy and convergence characteristics of the PDF method in complex flow configurations.



Figure 6. The computational grid of Combustor-B. Air is fed through swirlers and primary, dilution and effusion holes. The grid has 400,752 nodes.

Figure 7 presents the mixture fraction and temperature fields from the simulation. The overall fuel-air ratio of the flow is 0.0124. High temperatures are present in the primary zone, where the fuel-air mixture is within the flammability limits. Combustion is almost complete before the flow enters the secondary zone. The average mixture fraction at the exit of the combustor converges to the theoretical value of 0.0121 (fuel-air ratio = 0.0124).

Figure 8 shows the convergence behavior of mixture fraction and temperature at a fixed point in the flowfield. Note that large fluctuations are present in the field until 2000 iterations. Subsequently, the flowfield converges to a steady field. Also note that fluctuations are significantly higher in the mixture fraction field. Figure 9 presents the evolution of the total number of particles in the flowfield. Large fluctuations are seen in the number of particles before it settles to a steady value of 3.3×10^6 . This value corresponds to a 5% increase in the number of particles from the initial number of particles distributed in the flowfield.

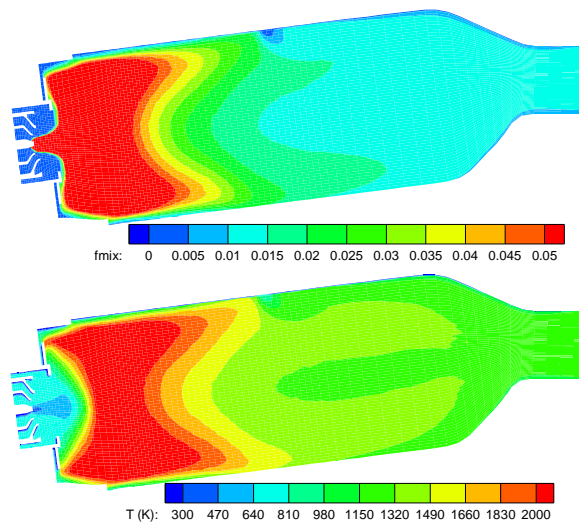


Figure 7. The mixture fraction (top) and temperature (bottom) fields from a simulation of Combustor-B with gaseous Propane fuel.

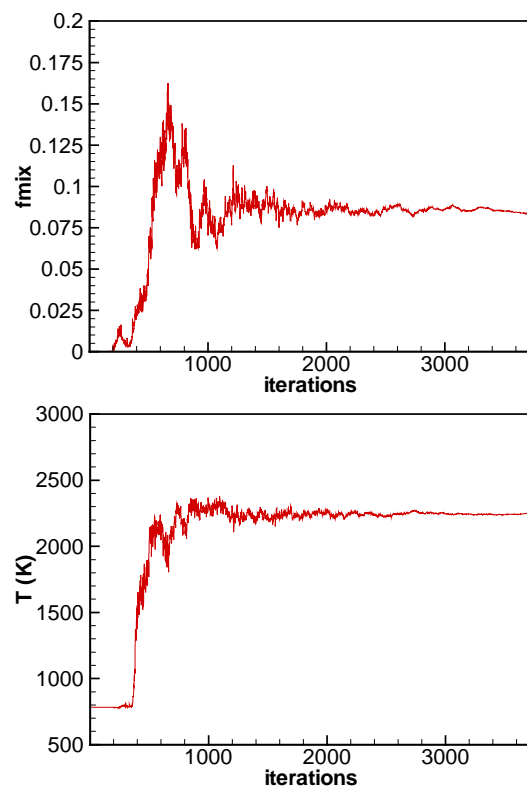


Figure 8. Convergence behavior of mixture fraction (top) and temperature (bottom) at a fixed point in the flowfield. Initial transients last until 2000 iterations.

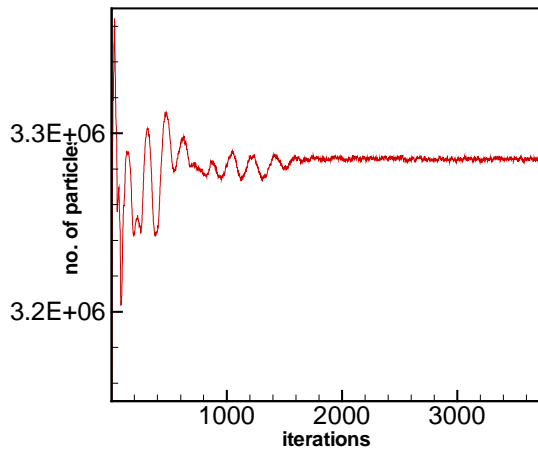


Figure 9. Evolution of the total number of particles in the flowfield. Large fluctuations are observed for the first 2000 iterations. Subsequently, the fluctuations are very small, indicating convergence of the flowfield.

A stringent test of the PDF algorithm is the linearity between mixture fraction and enthalpy that must be exhibited by the particle and mean fields for adiabatic gaseous fuel combustion. Figure 10 presents the relationship between the two physical quantities in both the particle and mean fields. As expected, a linear behavior is observed. The linearity in the particle field indicates that the interpolation algorithm and the particle cloning and clustering algorithm do not introduce spurious values. The same linear behavior is also seen in the mean fields.

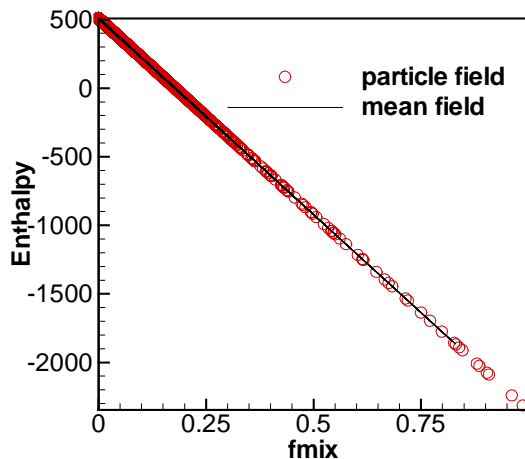


Figure 10. Relationship between mixture fraction and enthalpy in the particle (circles) and mean (line) fields. As expected, a linear behavior is seen.

Another test of the PDF algorithm is the consistency in density. Density can be computed via

two methods. The conventional method of computing density is through ensemble average of the density on each particle. Another method of computing density is by dividing the total mass in each cell by the volume of the cell. Figure 11 presents the density field using the two methods. It can be seen that the two fields are similar. A local accumulation of mass is seen at the stagnation points. This is not of concern, since one could block the stagnation regions and still obtain the same overall flowfield. A particle-position correction algorithm²² could be implemented to rigorously enforce the consistency condition. However, implementation of this algorithm in the present scalar PDF code has been postponed until further assessment of the universality of the constants used in the algorithm is performed

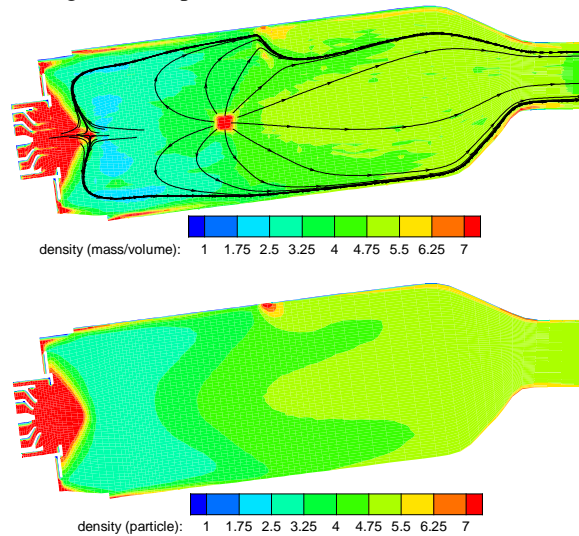


Figure 11. The consistency condition for density (Kg/m³). Top: Density computed from total mass of particles in a cell divided by the volume of the cell. Bottom: Density computed from conventional averages. Note that density from the two calculations is similar, except at the stagnation points.

Combustor-B is next simulated with liquid Jet A fuel. The airflows are kept the same as in the gaseous fuel case. The fuel is injected through nozzles on the dome. A simulation is performed until the average mixture fraction value at the exit converges to the expected value. Figure 12 presents the mixture fraction and temperature fields from the simulation. Note that the fuel evaporates in the primary zone, where high temperatures are observed. The dilution jets and effusion cooling air from the liner lowers the temperature in the secondary zone. Figure 13 presents the comparison of the burner exit temperature profile between predictions and measurements from a rig test of the combustor. Note that the predictions are in good agreement with rig data.

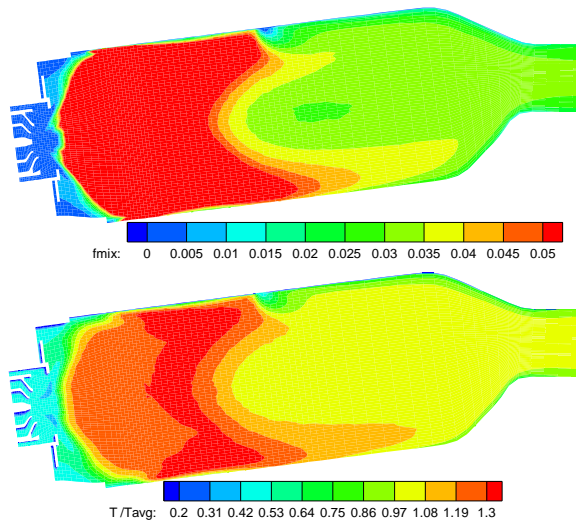


Figure 12. Mixture fraction (top) and temperature (bottom) fields from a simulation of Combustor-B with liquid Jet A fuel.

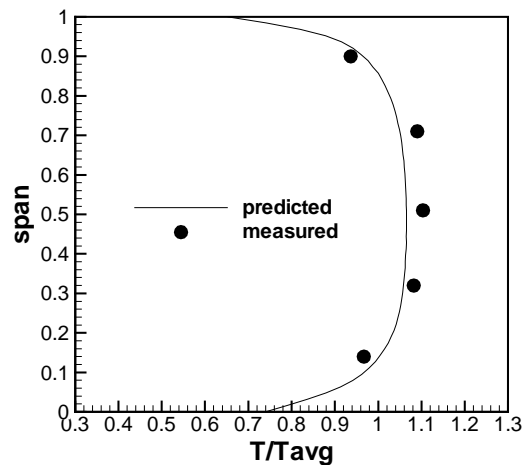


Figure 13. Comparison of predictions with rig measurements for the exit temperature profile in Combustor-B with liquid Jet A fuel.

Combustor-C

The PDF method has been used to simulate Combustor-C, which is a variant of Combustor-B with different flows and nozzle and hole geometry. The locations of the primary and dilution holes are different from those in Combustor-B. Figure 14 presents the grid for this combustor. Combustor-C is operated at a pressure of 14 atm and a temperature of 750 K. Liquid Jet A fuel is used in this combustor. A PDF simulation with 10 particles per cell is performed. Figure 15 shows the mixture fraction and temperature fields in the simulation. The average exit mixture fraction converges to the expected value. Figure 16 shows a comparison of predictions with measured data of the exit temperature profile. The predictions are in excellent agreement with rig data.



Figure 14. The grid on Combustor-C. A total of 400,752 nodes are used. PDF simulation is carried out with 10 particles per cell.

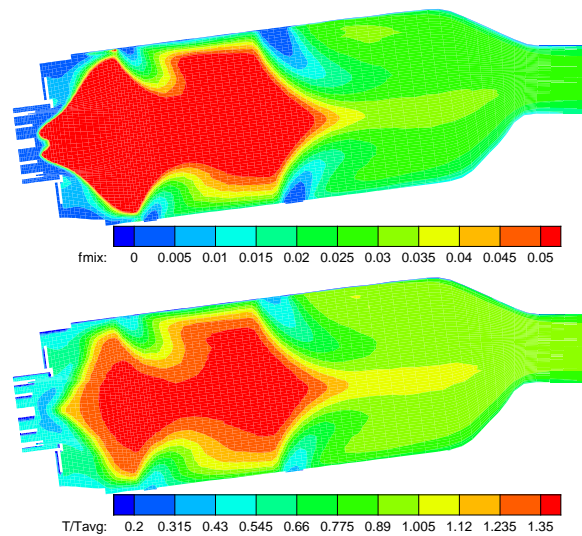


Figure 15. Mixture fraction (top) and temperature (bottom) in Combustor-C.

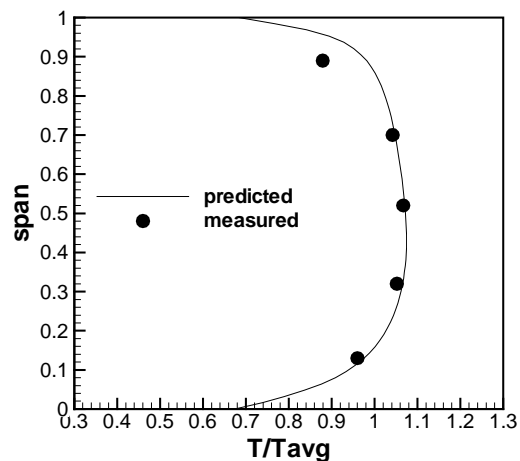


Figure 16. Comparison of predictions with rig measurements for the exit temperature profile in Combustor-C.

SUMMARY

The Lagrangian PDF transport method has been developed for the simulation of practical gas turbine combustor flows. The method involves an efficient particle tracking algorithm, a variable time-step method, and a conservative implementation of molecular mixing and spray evaporation. The method has been used in simulations of several combustors. Simulations of a model combustor with 10 and 60 particles per cell were performed. The simulations showed that statistical errors could be suppressed by time-averaging the fields computed from particles. Bias errors were observed to be not significant and as low as 10 particles per cell could be used to get reliable results. Simulations of an actual gas turbine combustor with gaseous Propane fuel were performed. This combustor is representative of actual combustors used in aircraft engines. Analyses of the results showed that the flowfield converged to the expected values and the expected linear behavior between mixture fraction and enthalpy in the particle field was obtained. The density field computed from particles as well as that computed using the mass in each cell was observed to be similar, indicating consistency between evolution of particles and the mean field. This combustor was also operated with liquid Jet A fuel and a simulation was performed. The predicted exit temperature profile was in good agreement with rig data. A similar combustor with different flowrates and different placement of the primary and dilution holes was also simulated. Again, the predicted exit temperature profile was observed to be in good agreement with rig data. The results indicate that the Lagrangian PDF transport method can be reliably used for the prediction of practical gas turbine combustor flows.

ACKNOWLEDGEMENTS

This work was funded in part by the Indiana State 21st Century Research Fund.

REFERENCES

1. Pope, S. B., "A Monte-Carlo Method for the PDF Equation of Turbulent Reactive Flow," *Combustion Science and Technology*, Vol. 25, No. 5, 1981.
2. Pope, S. B., "PDF Methods for Turbulent Reactive Flows," *Progress in Energy and Combustion Science*, 11, pp. 119, 1985.
3. Xu, J. and Pope, S. B., *Combust. Flame*, Vol. 123, pp. 281-307, 2000.
4. Anand, M. S., Takahashi, F., Vangsness, M. D., and Schmoll, W. J., "An Experimental and Computational Study of Swirling Hydrogen Jet Diffusion Flames," *Journal of Engineering for Gas Turbines and Power*, Vol. 119, pp. 305-314, 1997.
5. James, S., Anand, M. S., Razdan, M. K., and Pope, S. B., "In Situ Detailed Chemistry Calculations in Combustor Flow Analyses," *Journal of Engineering for Gas Turbines and Power*, Vol. 123, pp. 747-756, 2001.
6. James, S. and Anand, M. S., "Detailed Chemistry Calculations of Piloted Jet Diffusion Flames Using the PDF-ISAT Method," *Technical Meeting of the Central States Section of the Combustion Institute*, 2000.
7. James, S., Zhu, J. and Anand, M. S., "Simulations of Gas Turbine Combustor Flows Using the Node-Based PDF Transport Method," AIAA 2002-4013, *AIAA Joint Propulsion Conference*, July 2002.
8. Haworth, D. C. and El Tahry, S. H., *Seventh Symposium on Turbulent Shear Flows*, Stanford University, p. 13.1, 1989.
9. Mobus, H., Gerlinger, P., Bruggemann, D., "Comparison of Eulerian and Lagrangian Monte Carlo PDF Methods for Turbulent Diffusion Flames," *Combustion and Flame*, 124: 519-535, 2001.
10. Eggels, R. L. G. M. and Goey de, L. P. H., "Mathematically Reduced Reaction Mechanisms Applied to Adiabatic Flat Hydrogen Flames," *Combust. Flame*, Vol. 100, pp.559, 1995.
11. Pope, S. B., *Combust. Theo. Modelling*, Vol. 1, pp. 41-63, (1997).
12. Anand, M. S., Zhu, J., Connor, C., and Razdan, M. K., "Combustor Flow Analysis Using an Advanced Finite-Volume Design System," *ASME paper 99-GT-273*.
13. Zhu, J., "On the Higher-Order Bounded Discretization Schemes for Finite-Volume Computations of Incompressible Flows," *Computer Methods in Applied Mechanics and Engineering*, Vol. 98, pp. 345-360, 1992.
14. Dopazo, C. *Phys. Fluids*, 18, 397, 1975.
15. Jenny, P., Pope, S. B., Muradoglu, M., and Caughey, D. A., "A Hybrid Algorithm for the Joint PDF Equation of Turbulent Reactive Flows," *J. Comp. Phys.* 166, 281-252, 2001.
16. Muradoglu, M. and Pope, S. B., "A Local Time Stepping Algorithm for Solving the PDF Equations for Turbulent Reacting Flows," Submitted to *AIAA Journal*.
17. Westbrook, C. K., and Dryer, F. L., "Simplified Reaction Mechanisms for the Oxidation of Hydrocarbon Fuels in Flames," *Combustion Science and Technology*, Vol. 27, pp. 31-43, 1981.
18. Gosman, A. D., and Ioannides, E., "Aspects of Computer Simulation of Liquid Fueled Combustors," *Journal of Energy*, Vol. 7, No. 6, pp. 482-490, 1988.
19. Anand, M. S., "A Study of Particle-Laden Jet Flow by the PDF Method," AIAA 90-1856.

20. Chin, J. S. and Lefebvre, A. H., "Steady-State Evaporation Characteristics of Hydrocarbon Fuel Drops," *AIAA Journal*, Vol. 21, No. 10, Oct. 1983.
21. Xu, J. and Pope, S. B., "Assessment of Numerical Accuracy of PDF/Monte Carlo Methods for Turbulent Reacting Flows," *Journal of Computational Physics*, 152, pp. 192-230, 1999.
22. Muradoglu, M., Pope, S. B., and Caughey, D. A., "The Hybrid Method for the PDF Equations of Turbulent Reactive Flows: Consistency Conditions and Correction Algorithms," *J. Comp. Phys.* 172, 841-878, 2001.